Disrupting Cholesterol-FOXO3-KRT14 axis suppresses metastasis of triple-negative breast cancer

Jie Dong (dongjie@nju.edu.cn)
Medical School of Nanjing University
Lingkai Kong
Medical School of Nanjing University
Mao Xia
Medical School of Nanjing University
Jiwu Wei
Nanjing University

Article

Keywords: Cholesterol, triple negative breast cancer, metastasis, keratin 14, FOXO3a, Apolipoprotein A1, oncolytic virus

Posted Date: October 4th, 2021

DOI: https://doi.org/10.21203/rs.3.rs-877843/v1

Title: Disrupting Cholesterol-FOXO3-KRT14 axis suppresses metastasis of triple-negative breast cancer

Running title:

Forced cholesterol efflux inhibits metastasis of TNBC

Abstract

High metastatic propensity is a devastating challenge to effective therapy of solid tumors, including triple-negative breast cancer (TNBC). In this study, we performed a genome-scale screen and found that cholesterol homeostasis is essential for tumor progression in immunocompetent mice. In an orthotopic TNBC model, intracellular cholesterol promoted lung metastasis by sustaining the expression of keratin 14 (KRT14) and decreasing MHC II, which was indispensable for the cluster metastasis of TNBC. Mechanistic studies demonstrated that FOXO3a regulated the transcription of KRT14. FOXO3a recognized and directly bound to the promoter of KRT14 to inhibit its expression. Cholesterol disrupted the nuclear translocation of FOXO3a by sustaining its phosphorylation, which was regulated by IKK, one of the major upstream kinases of FOXO3a. Apolipoprotein A1 (ApoA1) increased cholesterol efflux and inhibited TNBC metastasis by regulating the IKK-FOXO3a-KRT14 axis. The recombinant adenovirus encoding ApoA1 (ADV-ApoA1) promoted cholesterol efflux, dampened metastasis, and prolonged survival in mice bearing TNBC. Finally, we provided preliminary data showing that high doses of ADV-ApoA1 were well tolerated in rhesus monkeys and Syrian hamsters injected both intravenously and hypodermically. Taken together, cholesterol promotes metastasis via the IKK-FOXO3a-KRT14 axis in TNBC, and facilitating cholesterol efflux from TNBC cells is a promising therapeutic strategy for TNBC clinical treatment.

Key words: Cholesterol, triple negative breast cancer, metastasis, keratin 14, FOXO3a, Apolipoprotein A1, oncolytic virus

Introduction

Triple-negative breast cancer (TNBC) has a high rate of distant metastasis, and targeted therapies are lacking. Epidemiological and large-scale gene sequencing studies have reported high heterogeneity within TNBC tumors and almost no common actionable targets[1-3]. Patients with this aggressive breast cancer subtype have poor overall survival, demanding further investigation into the factors driving the initiation and development of the disease[4-6]. With the prevalence of obesity, hyperglycemia, hyperlipidemia and hyperinsulinemia, metabolic disturbances are commonly developed resulting in an increased incidence of TNBC [7,8]. The potential metabolic abnormalities that promote the progression of TNBC include increased total cholesterol, circulating low-density lipoprotein (LDL) cholesterol, triglycerides (TGs), insulin and decreased high-density lipoprotein (HDL) cholesterol [9,10]. Previous studies showed that elevated cholesterol or LDL levels were associated with increased breast cancer recurrence and reduced disease-free survival [11,12], highlighting the critical role of cholesterol in the pathogenic process of TNBC. Nevertheless, the mechanisms by which aberrant cholesterol metabolism promotes TNBC progression are not yet fully understood. Cellular cholesterol homeostasis relies on two aspects: one is the cholesterol uptake or de novo synthesis via the mevalonate-cholesterol pathway and cholesterol efflux mediated by apolipoproteins. Among the various subtypes of apolipoproteins, apolipoprotein A1 (ApoA1) plays a pivotal role in cholesterol efflux by binding to cellular membrane-bound receptors, including ABCA1 and ABCG1[13]. Several previous studies employed statins, the intensive inhibitors of cholesterol biosynthesis, for breast cancer treatment; however, the beneficial effects are still inconclusive in TNBC [14-16]. There is an urgent need to develop more effective therapeutics to manipulate aberrant cholesterol in TNBC.

TNBC contains subtypes expressing either basal keratins, such as KRT5 and KRT14, or luminal keratins, such as KRT8 and KRT18 [17,18]. KRT14 is a structural constituent of the cytoskeleton and participates in the assembly of desmosomes and hemidesmosomes as a major intermediate filament. KRT14 is considered a regulator of cell-cell and cell-extracellular matrix interactions. Breast cancer cells can propagate positive KRT14 ($KRT14^+$) and KRT14-negative daughter cells via asymmetric division and thereby generate heterogeneity [19]. A previous study showed that $KRT14^+$ breast cancer cells located at the invasion front or interface between the tumoroid and extracellular collagen and mediated collective dissemination[20]. $KRT14^+$ breast cancer cells exhibited more invasiveness in three-dimensional organoid assays and an enhanced ability to develop circulating tumor cell clusters, which showed a 100-fold increase in metastatic clone formation in vivo, compared with single tumor cells. Although only a small percentage of luminal tumors display basal epithelial gene signature, knockdown of KRT14 is sufficient to suppress collective invasion. However, the molecular mechanisms regulating KRT14 expression are still unclear, and the relationship between cholesterol and KRT14 is still unknown.

Forkhead box O3 (FOXO3a) is a member of the Fox transcription factor family, which is characterized by an evolutionarily conserved winged-helix DNA-binding motif at the N-terminal region [21,22]. FOXO3a is one of the human longevity genes and is beneficial for health and combating aging [23]. The target genes under the regulation of FOXO3a are involved in various physiological and pathological processes, including cell proliferation, cell cycle progression, apoptosis, survival, DNA damage and carcinogenesis [24-28]. FOXO3a is among the few longevity-associated genes in worms, flies and mammals [29]. Deregulation of FOXO3a is strongly associated with multiple malignancies, such as breast cancer, prostate cancer, acute myeloid leukemia, colon cancer, lung cancer and glioma [30]. Artificial manipulation of FOXO3a activity is a promising approach for cancer therapy. Phosphorylation is the primary mechanism

in modulating FOXO3a activity. When phosphorylated, FOXO3a is detained in the cytoplasm and then ubiquitinated and degraded by the proteasome [31].

Several upstream kinases, such as Akt, ERK, SGK, IKKβ and IKBKE have been reported to be able to phosphorylate FOXO3a[32]. The phosphorylation sites of FOXO3a are distinct for each kinase, e.g., at T32, S253, and S315 for Akt, S294, S253 and S425 for ERK, and S644 for IKK [33]. In fact, the overexpression of FOXO3a in breast cancer leads to upregulation of cyclin-dependent kinase inhibitors and displays a significant inhibition of tumor growth [34]. The sequestration of FOXO3a in the cytoplasm appeared to be associated with poor survival of patients with breast cancer [35]. The relationship between FOXO3a and the invasiveness/metastasis of TNBC and the role of cholesterol in regulating FOXO3a are not yet known.

In the current study, we investigated the mechanisms of cholesterol in promoting metastasis and invasiveness of TNBC and unveiled a novel pathway by which FOXO3a regulates KRT14. We also investigated a novel therapeutic approach using an oncolytic adenoviral vector encoding ApoA1 to inhibit the invasiveness and metastasis of TNBC.

Results

Imbalance in cholesterol metabolism promotes the progression and metastasis of TNBC

We developed a genome-scale genetic screening approach to identify metabolic pathways that are essential for the development of TNBC in vivo. First, 4T1 breast cancer cells were engineered to express synergistic activation mediators (dCas9-VP64 and MS2-p65-HSF1). Then these cells were transfected with an sgRNA library (CRISPR-Pool SAM mouse library) containing 69,225 sgRNAs targeting 23,439 protein-coding genes and 491 control sgRNAs (nontargeting sgRNAs) [36]. Genetic modification was confirmed by sgRNA sequencing. Subsequently, these tumor cells were transplanted into animals. We collected the tumors on days 5 and 10, and compared the sgRNA library representation（**Figure 1a**). Inspection of the

list of genes targeted by sgRNAs with significant differences indicated that phospholipid transporter activity and cholesterol efflux were substantially involved in the progression of 4T1 breast cancer (**Figure 1b**). By analyzing the gene expression profile from the TCGA and GTEx datasets, we found that gene sets associated with cholesterol transport and efflux were decreased in breast cancer tissues compared with normal tissues, while the gene sets related to cholesterol biosynthesis showed the opposite expression pattern (**Figure S1a**). The expression of cholesterol homeostasis and biosynthesis was elevated more in TNBC than in other subtype tumors (**Figure S1b**). Further analysis showed that breast cancer patients with higher expression of cholesterol efflux-related genes ApoA1 or NR1H3 (also known as LXRa) seemed to have prolonged survival. Unexpectedly, the expression of the genes SREBF1, SREBF2 or HMGCR, the key mediators controlling cholesterol biosynthesis, did not influence survival (**Figure 1c**). In the 4T1 murine model, mice that received a high-fat or high-cholesterol diet displayed a > 3-fold increase in serum cholesterol and a > 6-fold increase in serum low-density lipoprotein (LDL) (**Figures 1d**). Moreover, both high-fat and high-cholesterol diets significantly promoted the development of TNBC and shortened the survival time of tumor-bearing mice (**Figure 1e**). Finally, high cholesterol was beneficial to the lung or liver metastasis of the 4T1 cells (**Figure 1f**). These data suggest that an imbalance in cholesterol metabolism plays a substantial role in the development and metastasis of TNBC.

Forced cholesterol efflux suppresses lung metastasis of TNBC

To elucidate whether intracellular cholesterol reduction can suppress the development of TNBC, we established the genetically modified 4T1 cells with stable overexpression of ApoA1 ($4T1^{ApoA1}$), the major constituent of HDL that mediates cholesterol efflux and reverse transport. The $4T1^{ApoA1}$ cells displayed a reduced accumulation of intracellular cholesterol, and an increased extracellular cholesterol level compared with the parental wild-type 4T1 ($4T1^{WT}$) cells (**Figure 2a**). Moreover, mice inoculated with $4T1^{ApoA1}$ showed increased serum HDL and

decreased cholesterol (**Figure S2a**). These data confirmed that ApoA1 overexpression functionally mediated cholesterol efflux. Next, we found that overexpression of ApoA1 significantly suppressed 4T1 tumor growth and significantly prolonged survival (**Figure 2b and S2c**). Surprisingly, compared with the mouse burden with $4T1^{WT}$, robustly reduced lung metastatic nodes were observed in the mice bearing $4T1^{ApoA1}$ (**Figure 2d-f**). We further confirmed this observation by microCT analysis, which showed that overexpression of ApoA1 in 4T1 cells steadily inhibited the lung metastasis (**Figure S2b**). Three-dimensional culture results showed that ApoA1 overexpression significantly attenuated the collective budding and invasion of 4T1 cells (**Figure 2g**). Consistently, impaired migration and invasion were observed in $4T1^{ApoA1}$ cells in the wound-healing and Transwell chamber assays (**Figure 2h, i and S2d**). Notably, overexpression of ApoA1 did not affect cell proliferation (**Figure S2e**). Taken together, these results indicated that ApoA1 could suppress the lung metastasis of TNBC by promoting cholesterol efflux.

Forced cholesterol efflux inhibits lung metastasis of TNBC by downregulating the expression of KRT14

We further investigated the molecular mechanisms of suppressed lung metastasis of TNBC mediated by cholesterol efflux. Transcriptome analysis revealed that KRT14 was dramatically downregulated in $4T1^{ApoA1}$ compared with $4T1^{WT}$ (**Figure 3a**). Gene set enrichment analysis (GSEA) of differentially expressed genes showed that higher mRNA levels of genes associated with desmosomes were observed in $4T1^{WT}$ than in $4T1^{ApoA1}$ (**Figure 3b and c**), which was consistent with a previous report that KRT14 expression was correlated with desmosome adhesion complex genes [37]. Analysis based on the TCGA dataset indicated that the expression of KRT14 was higher in TNBC than in non-TNBC tumors (**Figure 3d**). Consistently, overexpression of ApoA1 in murine (4T1) and human (HCC1937) TNBC cell lines significantly reduced KRT14 expression (**Figure 3e**). Moreover, massively reduced expression

of KRT14 was observed in primary tumor tissues from mice bearing $4T1^{ApoA1}$ (**Figure 3f**). Since the cholesterol efflux mediated by ApoA1 is ABCA1 receptor-dependent, we next blocked ABCA1 using its antagonist disulfonic acid hydrate disodium salt (DIDS) and found that the presence of DIDS mitigated the downregulation of KRT14 in $4T1^{ApoA1}$ cells (**Figure 3g**). Moreover, knockdown of ABCA1 expression by shRNA also reversed the downregulation of KRT14 in ApoA1-overexpressing 4T1 cells (**Figure 3h**). To elucidate whether the downregulation of KRT14 mediated by ApoA1 is cholesterol-dependent, we evaluated the expression of KRT14 in 4T1 cells cultivated in medium supplemented with additional cholesterol. As expected, the presence of a high level of cholesterol obviously upregulated the expression of KRT14 (**Figure 3i**). Elevated expression of KRT14 was also observed in tumor tissue from the mice fed a high-fat or high-cholesterol diet (**Figure 3j**). We further investigated the survival of the mice challenged with KRT14 knockdown 4T1 cells ($4T1^{KRT14\text{-}KD}$). Indeed, a significantly prolonged lifespan and impaired lung metastasis were observed in mice bearing $4T1^{KRT14\text{-}KD}$ tumor cells compared to 4T1 cells ($4T1^{Ctr}$) (**Figure 3k-n**). In contrast, the re-expression of KRT14 in $4T1^{ApoA1}$ restored cell migration (**Figure 3n**). These results suggest that cholesterol in TNBC promotes invasion and metastasis by sustaining KRT14 expression, and cholesterol efflux can inhibit lung metastasis of TNBC by downregulating the expression of KRT14.

FOXO3a is a potential transcriptional regulator of KRT14

We further investigated the underlying mechanisms by which cholesterol efflux regulats the expression of KRT14. We found that the administration of either inhibitors of the proteasome MG132 or autophagosome chloroquine (CQ) did not affect the expression of KRT14 (**Figure S3a**), which excluded the regulatory roles of the two major protein degradation pathways. Then, we found that overexpression of ApoA1 induced a dramatic decrease in KRT14 mRNA levels, suggesting that AopA1-mediated cholesterol efflux altered the transcription of KRT14 (**Figure**

4a). Transcript factors, e.g., AP-1, AP-2, EST, SP1/SP3 and ΔNp63 have been reported to enhance KRT14 expression [38-40]. By analyzing the RNA sequencing data, we found that the expression of these transcription factors was comparable between $4T1^{ApoA1}$ and $4T1^{WT}$. Therefore, we switched to identify the potential transcription factors that suppress KRT14. CCAAT Enhancer Binding Protein (C/EBP) α and β have been reported to inhibit KRT14 expression by promoting nuclear translocation of nuclear factor of activated T cells 1 (NFATc1) in keratinocytes [41]. However, cholesterol altered by ApoA1 did not influence the nuclear level of NFATc1 in 4T1 cells (**Figure S3b**). Similarly, knockdown of (C/EBP) α or β in 4T1 cells did not affect the nuclear translocation of NFATc1 and KRT14 (**Figure S3b and c**). These data suggested that some yet undefined inhibitory transcription factors of KRT14 were regulated by cholesterol metabolism. Subsequently, we screened the top 10 suppressive transcription factors with differential expression between $4T1^{ApoA1}$ and $4T1^{WT}$. Knockdown of FOXO3a, double PHD fingers 2 (DPF2), KLF16 or Smad4 abrogated the ApoA1-induced decrease in KRT14 (**Figure 4b**). Nevertheless, robustly reversed expression of KRT14 was observed only in FOXO3a-silenced $4T1^{ApoA1}$ cells. Consistently, FOXO3a silencing in $4T1^{ApoA1}$ cells increased KRT14 at the protein level (**Figure 4c**) and led to improved cell migration (**Figure 4d**). In addition, GSEA enrichment revealed that the downstream genes positively regulated by FOXO3a were upregulated, whereas the downstream genes negatively regulated by FOXO3a were downregulated in $4T1^{ApoA1}$ compared with $4T1^{WT}$ (**Figure S3d**). These findings suggested that cholesterol metabolism regulated FOXO3a function, while ApoA1-mediated cholesterol reduction enhanced the transcription-modulating activity of FOXO3a. Further analysis of the TCGA dataset showed decreased mRNA expression of FOXO3a in a series of malignant tissues, including breast cancer, cervical squamous cell carcinoma and endocervical adenocarcinoma, lung adenocarcinoma, ovarian serous cystadenocarcinoma and skin cutaneous melanoma, compared with normal tissues (**Figure 4e and S4**). To clarify the

precise motif of the KRT14 promoter recognized by FOXO3a, we constructed a series of truncated KRT14 promoter-luciferase reporter vectors. The results showed that the region −800 to −2000 base pairs (bp) upstream of the transcriptional initiation site was essential for KRT14 transcription inhibition (**Figure 4f**). Four FOXO3a binding motifs are expected in the region -800 to -2000 bp of the KRT14 promoter. Luciferase assays showed that mutation of the binding site at -872 to -879 dampened the suppressive effect of FOXO3a on KRT14 transcription (**Figure 4g**). We further performed chromatin immunoprecipitation with the an antiFOXO3a antibody, and confirmed that the transcription factor FOXO3a directly conjugated to the KRT14 promoter (**Figure 4h**). Finally, we collected 100 tumor tissues from patients with biopsy-proven breast cancer, and analyzed the expression of both KRT14 and FOXO3a by immunohistochemistry. An inverse correlation was observed between the expression of KRT14 and FOXO3a (**Figure 4i and j**). Moreover, FOXO3a exhibited a positive correlation with serum ApoA1 and HDL levels (**Figure 4j**).

Taken together, these findings suggested that FOXO3a might be a pivotal suppressor of KRT14 by directly binding to its promoter, while ApoA1 mediated cholesterol efflux enhanced the transcription-modulating activity of FOXO3a.

Cholesterol efflux promotes the nuclear translocation of FOXO3a in an IKKβ phosphorylation-dependent manner

A previous study showed that FOXO3a could be phosphorylated at distinct sites and sequestered in the cytoplasm[42]. We further investigated whether ApoA1-induced cholesterol efflux influenced the FOXO3a phosphorylation. Overexpression of ApoA1 in both 4T1 and HCC1937 cells increased the nuclear level of FOXO3a (**Figure 5a**). Subsequently, we detected the upstream signaling of FOXO3a phosphorylation. As a result, overexpression of ApoA1 promoted the activation of the Akt pathway, and did not lead to any change at the Akt phosphorylation site (S315) of FOXO3a. In contrast, ApoA1 significantly suppressed the

activation of the Ikappa-B pathway (**Figure 5b**). Furthermore, an inhibited Ikappa-B signaling was also observed in tumor tissue from mice inoculated with $4T1^{ApoA1}$, compared with mice that received $4T1^{WT}$ cells (**Figure 5c**). Consistently, we found that the mRNA expression of IKK complex components, such as IKBKB, IKBKE and IKBKG, was significantly decreased in $4T1^{ApoA1}$ cells (**Figure 5d**). Consistently, supplementation with IKBKB in $4T1^{ApoA1}$ cells significantly upregulated the KRT14 expression (**Figure 5e**). To further identify which kinase exactly phosphorylated FOXO3a in the current experimental setting, we generated three plasmids with mutations in Akt, ERK or IKKβ phosphorylation sites. Only the mutation in the IKKβ phosphorylation site led to a comparable level of nuclear FOXO3a between wild-type and ApoA1-overexpressing 4T1 cells, indicating that the ApoA1-mediated FOXO3a dephosphorylation in 4T1 cells predominantly depended on the IKKβ pathway (**Figure 5f**). These results suggested that phosphorylation of FOXO3a induced by IKKβ was involved in the cholesterol-mediated regulation of KRT14 in TNBC. ApoA1-mediated cholesterol efflux reduced IKKβ expression, which in turn promoted the dephosphorylation and nuclear translocation of FOXO3a, eventually leading to the suppression of KRT14 transcription.

Replicative adenoviral vector-based ApoA1 gene therapy substantially inhibited tumor progression

Having shown that overexpression of ApoA1 in TNBC inhibited tumor growth and metastasis, we sought to investigate the antitumor efficacy of ApoA1-based gene therapies. We constructed ApoA1-overexpressed oncolytic adenovirus (ADV-ApoA1) (**Figure S5a**), adeno-associated virus (AAV-ApoA1) and vaccinia virus (VV-ApoA1). We found that ADV-ApoA1 treatment reduced tumor growth and prolonged the survival of 4T1-bearing mice (**Figure 6a**), while AAV-ApoA1 showed mildly prolonged survival with no inhibition of tumor growth (**Figure 6b**). Surprisingly, VV-ApoA1 did not show any antitumor efficacy in 4T1-bearing mice (**Figure S5b**). In addition, we confirmed that ADV-ApoA1-infected cells produced and

secreted a large amount of ApoA1 protein (**Figure S5c**), and ADV-ApoA1 displayed comparable replication capacity compared with control adenovirus (ADV-Ctr) (**Figure S5d**). To investigate whether ADV-ApoA1 could inhibit the metastasis of TNBC *in vivo*, we performed a biodistribution assay using luciferase-labeled 4T1 cells. We found that lung metastases were significantly reduced in 4T1-bearing mice treated with ADV-ApoA1 (Figure 6c). Consistently, ADV-ApoA1 significantly reduced the expression of KRT14 in 4T1- bearing mice (**Figure 6d**). Similarly, ADV-ApoA1 also significantly decreased the expression of KRT14 in 4T1 cells *in vitro* (**Figure 6e**). Moreover, in a nude mouse model bearing orthotopically implanted human TNBC cells (MDA-MD-231), administration of ADV-ApoA1 suppressed lung metastases and prolonged the lifespan of the mice (**Figure S5e and S5f**). Furthermore, the expression of EMT-related genes including snail, vimentin and slug, were upregulated in the tumor tissues isolated from the mice treated with ADV-Ctr and was not increased in mice treated with ADV-ApoA1 compared to those treated with saline (**Figure S5g**). Interestingly, we found that overexpression of adenovirus early region 1 (E1A) in HCC1937 and 4T1 cells significantly increased the expression of ABCA1, the specific receptor mediating ApoA1-induced cholesterol efflux (**Figure 6f**). As KRT14 expression was reported to be involved in MHC class II presentation in breast cancer[37] we therefore evaluated the immune microenvironment in tumor tissue. We found that mice that received ADV-ApoA1 treatment displayed upregulated $CD4^+$ T cells with granzyme K expression (CD4.GZMK) or cytotoxic CD4+ T cells (CD4. Cytotoxic) in tumor tissue (**Figure 6g**). GSEA revealed that ADV-ApoA1 treatment induced enhanced MHC class II process signaling (**Figure 6h**), and $4T1^{ApoA1}$ displayed elevated MHC class II molecules, compared with $4T1^{WT}$ (**Figure 6i**). Consistently, MHC class II expression was increased in $4T1^{ApoA1}$ compared with $4T1^{WT}$, while MHC class I levels were parallel between $4T1^{ApoA1}$ and $4T1^{WT}$ (**Figure 6j**). In addition to TNBC, we further investigated and observed the effective therapeutic outcomes of ADV-

ApoA1 on other types of solid tumors, including lung cancer (LLC), pancreatic cancer (Pan02) and colorectal cancer (C26) (**Figure S5h**).

Regarding the improved permission for adenovirus replication in humans, we evaluated the preclinical safety of ADV-ApoA1 in two other species, rhesus monkeys and Syrian hamsters. The dose range-finding (DRF) in Syrian hamsters was 5×10^{12} VP (viral particles)/kg for hypodermic injection (I.H.) and 1.2×10^{12} VP/kg for intravenous injection (I.V.) for 10 viral injections within 12 days (**Table 3**). The maximum toxic dose (MTD) in rhesus monkeys by I.H. or I.V. was 1×10^{13} VP/kg for only one injection, and DRF in rhesus monkeys was 5×10^{12} VP/kg for I.H. and 2.4×10^{11} VP/kg for I.V., respectively, for 10 viral injections within 12 days (**Table 4**). All animals survived under the administration of ADV-ApoA1 and did not show any tendency to consume less food or weight loss than the vehicle control group did. No significant differences in hematological parameters, such as WBC, neutrophil, or monocyte counts, were observed between the vehicle and treatment groups. Only moderate elevated levels of ALT (125.0 ± 16.0 U/L vs 33.6 ± 13.6 U/L in monkeys prior to viral injection) were observed in rhesus monkeys that received ADV-ApoA1 by I.V. at a dose of 1×10^{13} VP/kg (**Table 4**).

Taken together, these results indicated that adenovirus vector-based ApoA1 gene therapy substantially suppressed the lung metastasis of TNBC by reducing KRT14, and ADV-ApoA1 showed good safety in both Syrian hamsters and rhesus monkeys.

Discussion

TNBC, a highly aggressive subtype of breast cancer, is a difficult disease to treat in the clinic. It is resistant to targeted therapeutic approaches, and the backbone of therapy against TNBC with various clinicopathologic features remains cytotoxic chemotherapy, resulting in unsatisfactory clinical outcomes [43]. In the current study, we delineated the roles and the mechanisms of cholesterol in the progression and metastatic characteristics of TNBC. For the

first time, we identified the cholesterol/IKK/FOXO3a/KRT14 axis that regulated the remote metastasis of TNBC and further provided an oncolytic adenovirus expressing ApoA1 that effectively enhanced cholesterol efflux, resulting in inhibition of TNBC (**Figure 6k**).

By performing genome-scale screening of multiple diverse biological processes, we found that cholesterol metabolism was essential for tumor development. Indeed, a high-fat diet, particularly a high cholesterol diet, significantly promoted the progression and metastasis of TNBC in a murine model. Furthermore, we found that the expression of ApoA1 and NR1H3, which are involved in cholesterol efflux, was positively related to the survival time of patients with breast cancer. Currently, cholesterol biosynthesis is the mainstay therapeutic target for hypercholesterolemia [44]. Several studies have shown that statins are potential agents for cancer treatment by reducing cholesterol biosynthesis; however, the beneficial effect of statins on cancer incidence and mortality has not yet been fully confirmed [45]. Little is known about its antitumor efficacy by facilitating cholesterol efflux. In this study, we showed that elevated cholesterol efflux mediated by enforced expression of ApoA1 significantly reduced the metastases and prolonged the lifespan of mice bearing TNBC. Therefore, our study provides some evidence that cholesterol efflux can also be recruited for cancer therapy by targeting cholesterol-related cancers.

Accumulating studies have suggested that cholesterol contributes to TNBC metastasis [46]. However, the underlying mechanisms are largely unknown. Several studies have shown that KRT14 mediates the collective dissemination of TNBC and is considered to be one of the specific markers of invasive basal-like breast carcinomas [37,47,48]. However, the regulatory mechanisms of KRT14 in TNBC remain to be clarified. In the current study, we identified a correlation between cholesterol and KRT14 in TNBC, e.g., KRT14 was significantly upregulated in the presence of high cholesterol, whereas it was markedly reduced by ApoA1-

mediated cholesterol efflux and therefore significantly reduced cell migration, invasion and metastases in TNBC.

We found that cholesterol transcriptionally altered the expression of KRT14 but not the expression of KRT14 posttranslationally. After screening the transcription factors that have been reported to control KRT14 expression, cholesterol seemed to promote KRT14 transcription mainly in a previously unknown signaling pathway. For the first time, we identified that the transcription factor FOXO3a regulated by cholesterol was a specific repressor of KRT14. FOXO3a has been reported to function by recognizing and binding to the DNA motif 5'-[AG]TAAA[TC]A-3' [49-51]. We found that there existed a specific conjugation between FOXO3a and the KRT14 promoter region, and there were several FOXO3a recognizing DNA motifs in the 1–2000 bp upstream of the KRT14 transcription initiation site and that -872 to -879 bp in the KRT14 promoter was the exact DNA binding motif for FOXO3a. Therefore, cholesterol orchestrates KRT14 expression by suppressing the regulatory function of FOXO3a. In agreement with our findings, we further confirmed an inverse correlation between the expression of KRT14 and FOXO3a in breast tumor tissues from patients.

Previous studies showed that FOXO3a was regulated mainly by the PI3K/Akt, ERK, and IKK signaling pathways, and the phosphorylation of FOXO3a influences its nuclear translocation of FOXO3a [35,46,52]. We found that the cytoplasmic retention of FOXO3a controlled by cholesterol was mainly through the IKK signaling pathway, rather than through the PI3K/Akt or ERK signaling pathways. Our finding is consistent with a previous study, which showed that IKK-mediated negative regulation of FOXO3a was a key mechanism for cell growth and tumorigenesis of breast cancer [35]. Therefore, cholesterol may be a substantial factor to sustain the activity of IKK signaling, and ApoA1-induced cholesterol efflux dramatically reduced IKK components leading to increased nuclear translocation of FOXO3a.

To answer the question of whether ApoA1-mediated cholesterol efflux would inhibits TNBC progression, we employed the viral vectors, including VV, AAV and ADV, to express ApoA1. Interestingly, ADV-ApoA1 treatment was more effective in both primary tumor control and lung metastasis inhibition than the VV-ApoA1 or AAV-ApoA1 intervention. AAV-ApoA1 showed less efficacy than ADV-ApoA1 in the inhibition of primary tumor growth of TNBC, possibly due to the nonreplicative nature of the AAV vector and insufficient ApoA1 production. Surprisingly, we did not observe any antitumor effect in mice that received VV-ApoA1 treatment. A possible explanation is that VV contains several envelope proteins, and it has been shown that cholesterol is required for the binding process between viral envelope proteins and lipid rafts, which is crucial for VV entrance into host cells [53]. However, replication-competent ADV-ApoA1 infected and replicated in cancer cells and subsequently expressed and produced ApoA1 within the tumor microenvironment, resulting in sufficient cholesterol efflux. Of note, the E1A protein that was produced during ADV replication significantly upregulated the expression of ABCA1, a membrane-bound receptor required for ApoA1-mediated cholesterol efflux. This feature makes replicative ADV an optimal vector for ApoA1-mediated cholesterol efflux in cancer therapy. Indeed, in addition to inhibiting TNBC, ADV-ApoA1 also displayed significant antitumor effects in mice bearing subcutaneous lung cancer or colorectal carcinoma. To evaluate the biological safety of ADV-ApoA1 for future clinical application, we further investigated the systemic toxicology of ADV-ApoA1 in two other species, rhesus monkeys and Syrian hamsters, and the preliminary data obtained in preparation for a phase 1 clinical trial showed the satisfactory safety of ADV-ApoA1. Notably, there were no detectable abnormalities in either animal when ADV-ApoA1 was injected 10 times every day for 12 days, even at a dose 8–10-fold that of the estimated high dose required for patients.

In the current study, we found that MHC-II expression is upregulated in KRT14-reduced TNBC, consistent with a previous study showing that KRT14 was correlated with MHC class

II antigen presentation protein complexes (MHC-II) in TNBC [37]. Given that MHC-II expression determines the activation of CD4+ T cells [54-57] and/or its downstream effect, e.g. CTL priming by antigen cross-presentation, our results suggest that manipulation of cholesterol efflux is not only sufficient to inhibit TNBC metastases, but may also promote an antitumor immune microenvironment. Therefore, apart from immune checkpoint inhibitors (ICIs), metabolism modulation such as cholesterol reduction in the TME, is a plausible therapeutic strategy for immune cell reinvigoration. Furthermore, the combination of ADV-ApoA1 and ICIs might exert a synergistic antitumor effect, which is worthy of further exploration.

In summary, the current study reveals a molecular axis, cholesterol-IKK-FOXO3a-KRT14, by which cholesterol promotes metastasis in TNBC. FOXO3a is a transcription repressor of KRT14. ApoA1-mediated cholesterol efflux effectively reduces the phosphorylation of FOXO3a by IKK leading to nuclear translocation of FOXO3a and consequently suppressing KRT14 transcription. Replicative ADV-ApoA1 infection elevates ABCA1 and facilitates the ApoA1-mediated cholesterol efflux. ADV-ApoA1 gene therapy displays good safety and improved antitumor outcomes in both tumor progression and lung metastases. ADV-ApoA1 is a potent antitumor biological agent that is worthy to be tested in further clinical studies.

Methods

Cell lines

The cell lines used in this study included 293T (human embryonic kidney cell), HCC1937, MDA-MB-231(Human triple negative-breast carcinoma), 4T1 (mouse mammary carcinoma cell), A549 (Human non-small cell lung cancer cell) and Hela-S3 (Human cervix carcinoma cell) were obtained from the American Type Culture Collection (ATCC; USA). Cells were cultured in Dulbecco's modified Eagle's medium (DMEM, Gibco-Thermo Fisher Scientific, USA) supplemented with 10% fetal bovine serum (FBS, Gibco). 293T cells were cultured in suspension in serum-free medium (Basalmedia, Shanghai, China) in spinner flasks (Jetbiofil,

Guangzhou, China). All cells were incubated at 37 °C with 5% CO_2 atmosphere. 4T1 and HCC1937 with ApoA1 over-expression were generated after lentiviral transduction and puromycin selection.

CRISPR screening in 4T1 tumor cells in vivo

The Genome-scale CRISPR-Cas9 transcriptional activation screening was described previously [36,58]. Briefly, the lentiviruses used to establish the transcription activation system were purchased from Genechem Company (Shanghai, China). Mouse CRISPR 3-plasmid activation pooled library (SAM) was a gift from Feng Zhang (Addgene #1000000075). A dCas9-VP64 fusion and MS2-p65-HSF1 expressing version of the 4T1 cell line was generated. Concentrations for selection agents were determined using a kill curve: 10 μg/ml blasticidin, and 200 μg/ml hygromycin. Cells were replated at low density (1 × 107 cells per T225 Flask) and the Lenti-sgRNA library was added at a MOI of 0.5. 48h later, cells were selected in the presence of 2 μg/ml puromycin. Genomic DNA was prepared from half of the cells and PCR was used to amplify the sgRNA region. The PCR production was used for sequencing on Illumina HiSeq to determine sgRNA transduction efficiency.

The genome-scale screening in vivo was performed according to the previous publication [59]. 4T1 cells containing transcription activation system were subcutaneously injected into BALB/c mice(n=6). On days 5 and 10, mice were scarified (n=3 for each time point) and tumors were collected for genomic DNA extraction. PCR was used to amplify the sgRNA region. The PCR productions were sequenced on an Illumina HiSeq to determine sgRNA abundance. Significantly enriched or depleted sgRNAs in the comparison of different time points were identified according to the previous report [60].

Cholesterol analysis

Cholesterol was measured with a cholesterol efflux assay kit (Biovision, CA, USA). Cells were seeded in a 96-well tissue culture plate using a 100 μl growth medium per well. Labeling

medium were prepared by mixing Labeling Reagent and serum-free RPMI medium. Cells were incubated in the labeling medium for 1h. The the medium was replaced by an equilibration medium and incubate the plate overnight. Aspirate the medium and add 2% LDL/VLDL-depleted cholesterol acceptors diluted in phenol red-free, serum-free RPMI medium. The plate was incubated for another 4h, then the fluorescence intensity (RUF) of supernatant and cell lysis were measured (Ex/Em = 485/523 nm). Cholesterol efflux was determined using the formula: Cholesterol efflux= [RUF(supernatants)/RUF(supernatants+cells)] ×100%.

Transwell assays

Transwell assay was performed with 8 μm pore-size Transwell chambers (Corning, NY, USA). The Transwell insert membrane was coated by rat tail type I collagen (Corning, NY, USA). The cells were cultured in a complete medium at 37 °C in 5% CO2 for 24 h. Then the cells on the upper surface of the insert membrane were gently removed with cotton swabs, and then the cells on the lower surface of the membrane were stained using methanol and 0.1% crystal violet solution. Invaded cells were observed and photographed with a microscope (Olympus, Tokyo, Japan). Five visual fields (magnification, ×100) were selected randomly for each chamber.

Wound healing assays

Cells were seeded in 12-well dishes (5 × 104 cells/well), and incubated in DMEM medium without FBS. When reaching a confluence of 80%, the cells were scratched across the surface of the well by a 10-μl pipette. After incubation, the scratches were observed at indicated time points.

Immunohistochemistry (IHC)

Tumor tissues were fixed with 4% paraformaldehyde and sectioned into 5-μm-thick slides. Primary antibody against p65 (Cell Signaling Technology, Danvers, MA, USA) was used for incubation at 4°C overnight. Then the slides were incubated with HRP-conjugated streptavidin for 1 h at room temperature. DAB chromogen (Zhongshan Golden Bridge, Beijing, China) was

used for visualization. Images were captured by a microscope (Zeiss, Oberkochen, Germany) at × 100 or × 400 magnifications.

Three-dimensional matrigel culture

Three-dimensional matrigel culture was described previously[61]. Briefly, a 20ul medium droplet containing 100 cells was cultured on the lower surface of the dish cover overnight. Then the droplets were seeded on the matrigel gel (Corning, NY, USA). Following a growth period, images were taken at 10 × objectives using an inverted microscope.

Replication of the oncolytic adenovirus in tumor cells

4T1 cells were seeded in a 24-well plate at 5×10^4 cells per well and placed in a 5% CO2 incubator at 37 °C. After 90% confluence, cells were infected with recombinant oncolytic adenovirus at MOI of 0.1. The cells were harvested after 24, 48, 72, and 96 h and then disrupted by three freeze-thaw cycles, and centrifuged at 3000 × g for 10 min. The virus supernatants were collected for viral genome extraction. Virus copies were determined by a a quantitative real-time polymerase chain reaction (Q-PCR).

Recombinant oncolytic virus construction, purification, and expansion

Recombinant adenovirus and vaccinia virus were generated as previously described[62,63]. For the recombinant VV construction, the shuttle plasmid was synthesized by GenScript (Nanjing, China). HEK293 cells were infected with Western Reserve (WR) strain (ATCC VR-1354) at a multiplicity of infection (MOI) of 1 for 2 h and then transfected with control or ApoA1 coding shuttle plasmids. Infected HEK293 cells were cultured in the presence of 25 mg/ml mycophenolic acid (MPA; Cat# A600640, Sangon Biotech, Shanghai, China), 250 mg/ml xanthine (Cat# A601197, Sangon Bio-tech), and 15 mg/ml hypoxanthine (Cat# A500336, Sangon Biotech). After three cycles of screening, recombinant VVs were isolated by three cycles of plaque purification, and further expanded by Hela-S3 cells in 6-well plates, cell culture dishes, and cell culture spinner flasks.

For the recombinant ADV construction, the shuttle plasmid was synthesized by GenScript (Nanjing, China).In this plasmid, the reporter gene EGFP and adenovirus E1A gene are linked by a T2A peptide sequence and are under the control CMV promoter. EF1a promoter controlled the expression of ApoA1 (Table S1). The recombinant adenoviral vector expressing ApoA1 was obtained via homologous recombination between the shuttle plasmid and the adenovirus backbone pAd/PL-DEST (Thermo Fisher Scientific, Invitrogen, Carlsbad, CA, USA). After digestion with the restriction enzyme PacI, the linear recombinant adenoviral vector was used to transfect 293T cells using jetPEI transfection reagent (Cat# 101-10N, Polyplus-transfection, France). The recombinant adenovirus was then amplified in 293T cells and purified using double cesium chloride gradient ultracentrifugation.

Virus titration was determined by adding serially diluted virus into a 96-well plate seeded with 293T cells or Hela-S3 (10,000 cells/well). Cells were cultured for 4 days, and fluorescence plaque was counted. The virus titer was calculated according to the following formula:

$TCID_{50} = 10^{2+(S/10-0.5)}$ /ml, pfu/ml=0.7×$TCID_{50}$ /ml, where S is the total number of fluorescence-positive wells, and N is the number of replicates.

The AAV-ApoA1 and negative control were purchased from OBiO Technology (Shanghai, China)

Western Blot Analysis

Cell culture medium was removed from the dishes and the cells were lysed in RIPA lysis buffer (Cell Signaling Technology, MA, USA) supplemented with a protease inhibitor cocktail (ThermoScientific, Waltham, MA). Supernatants from cell lysis were collected and mixed with loading buffer in the presence of 2-mercaptoethanol (2-ME) and heated at 95℃ for 5 min. After separation on a 10% SDS-PAGE gel, the proteins were transferred to a polyvinylidene fluoride (PVDF) membrane (Merck Millipore, MA, USA) and incubated with rabbit anti-KRT14 antibody (Abcam, Cambridge, UK), rabbit anti-FOXO3a antibody, anti-GAPDH, β-actin, anti-

phospho-Akt, anti-phospho-Ikb (Cell Signaling Technology),rabbit anti- histone H3.1 (Abmart, Shanghai, China), mouse anti-Flag (GenScript Biotech, Nanjing, China). After washing, the membrane was probed with horseradish peroxidase (HRP)-conjugated anti-mouse or rabbit IgG (GenScript Biotech, Nanjing, China) and visualized with western blot chemiluminescence reagent (GE Healthcare, Giles, UK) using an imaging system (Sage Creation Science, Beijing, China).

Immunofluorescence

For immunofluorescence staining, cells grown on poly-L-Lysine-coated coverslips were fixed with 4% PFA, permeabilized using 0.25% Triton-X. Cells were incubated with primary antibody: Rabbit anti-NFATc1 (Cell signaling technology) at 4 °C overnight, followed by incubation with AlexaFlour568 conjugated secondary antibody. Nuclei were counterstained with Hoechst 33258 (Beyotime Biotechnology, Shanghai, China). The primary antibody used for the frozen section of tumor tissue was the rabbit anti-KRT14 antibody (Abcam).

CHIP-seq analysis

Rabbit anti-FOXO3a antibody (#ab12162) from Abcam and Enzymatic Chromatin IP kit (Cell Signaling Technology) were used for the ChIP-Seq experiment. Briefly, 80% confluent $4T1^{ApoA1}$ cells were cross-linked with 1% formaldehyde at room temperature for 10 min. Chromatin was digested with Micrococcal Nuclease and sonicated to 100–500 bp. Then chromatin was digested with RNAse A and proteinase K, and incubated overnight with 4 μg of anti-FOXO3a antibody. ChIP DNA was magnetically purified with the column system. Eluted DNA was used for Chip-seq. The Chip-seq experiment and analysis were performed by Novogene (Beijing, China).

Q-PCR

Total RNA was extracted using Trizol (TRIzol, Invitrogen) following the manufacturer's instructions. After reverse transcription, Q-PCR was performed in QuantStudio 5 instrument

(Applied Biosystems). The oligonucleotide sequences of primers used for Q-PCR were reported in table 1. GAPDH was used as an internal reference and co-amplified with target samples using identical Q-PCR conditions. Samples were run in triplicate and mRNA expression was generated for each sample.

Animal models

Six-week-old female BALB/c mice were purchased from the Model Animal Research Center of Nanjing University (Nanjing, China). All animal experiments were performed following the guidelines that had been approved by the Animal Care and Use Committee of the Medical School of Nanjing University. For the VV and ADV therapeutic regime, 4T1 tumor cells were injected orthotopically into the fourth mammary glands. When the tumor reached 100 mm^3 (day0), the mice were randomly divided into different groups and treated with intratumoral (I.T.) injection of PBS or recombinant VV or ADV. In the AAV treated murine model, 4T1 tumor cells were injected subcutaneously (S.C.) into the right flank of the mice. PBS or AAV was injected S.C. on day 0 and day 7. Tumor length (L) and width (W) were measured every two days using Vernier calipers and the tumor size (V) was calculated by the following formula: $V = (L \times W^2)/2$. Mice were sacrificed if they had a tumor greater than 2000 mm^3 in volume.

Toxicity of ADV-ApoA1 in syrian hamster and rhesus monkey models

Syrian hamster and Rhesus monkey studies were carried out at the INNOSTAR company (Shanghai, China). Syrian hamsters (n = 120) were randomized by body weight into one of six groups comprised of 60 male and 60 female hamsters distributed in equal numbers. For MTD groups, the hamsters were treated by 2×10^{13} VP of ADV-ApoA1 I.H. or I.V. for once. For DRF groups, the hamsters were treated with 5×10^{12} VP or 1.2×10^{12} VP of virus I.H. or I.V. for five consecutive days. After two days rest, hamsters were treated with ADV-ApoA1 for another five consecutive days. Blood was collected 24h after the last viral injection for

hematology and clinical chemistry test. The experiment with Rhesus monkey (n=12) was similar. The medium was used as a negative control.

siRNA transfection

siRNAs were purchased from GenePharm (Shanghai,China). Cells were transfected with siRNA (100nM) for 48 or 72 h with Lipofectamine RNAi MAX Reagent (Thermo Fisher Scientific). The siRNAs used are shown as follows:

Statistical Analysis

All data were expressed as mean ± SD. One-way ANOVA analysis or student t-test were used to assess the differences between groups. Pearson correlation or Spearman correlation was adopted for correlation analysis. $P < 0.05$ was considered significant. All analyses were performed using the SPSS statistical software for Windows, version 19.0 (SPSS Inc., Chicago, IL, USA).

Declaration of Interests

The authors disclose no conflicts of interest.

References

1. Burstein, M.D.*, et al.* Comprehensive genomic analysis identifies novel subtypes and targets of triple-negative breast cancer. *Clin Cancer Res* **21**, 1688-1698 (2015).
2. Rody, A.*, et al.* A clinically relevant gene signature in triple negative and basal-like breast cancer. *Breast Cancer Res* **13**, R97 (2011).
3. Shah, S.P.*, et al.* The clonal and mutational evolution spectrum of primary triple-negative breast cancers. *Nature* **486**, 395-399 (2012).
4. Denkert, C.*, et al.* Tumour-infiltrating lymphocytes and prognosis in different subtypes of breast cancer: a pooled analysis of 3771 patients treated with neoadjuvant therapy. *Lancet Oncol* **19**, 40-50 (2018).
5. Waks, A.G. & Winer, E.P. Breast Cancer Treatment: A Review. *JAMA* **321**, 288-300 (2019).

6. Nunez Abad, M.*, et al.* Update on systemic treatment in early triple negative breast cancer. *Ther Adv Med Oncol* **13**, 1758835920986749 (2021).
7. Nelson, E.R.*, et al.* 27-Hydroxycholesterol links hypercholesterolemia and breast cancer pathophysiology. *Science* **342**, 1094-1098 (2013).
8. Crispo, A.*, et al.* Risk Differences Between Prediabetes And Diabetes According To Breast Cancer Molecular Subtypes. *J Cell Physiol* **232**, 1144-1150 (2017).
9. Yee, L.D., Mortimer, J.E., Natarajan, R., Dietze, E.C. & Seewaldt, V.L. Metabolic Health, Insulin, and Breast Cancer: Why Oncologists Should Care About Insulin. *Front Endocrinol (Lausanne)* **11**, 58 (2020).
10. Gallagher, E.J.*, et al.* Elevated tumor LDLR expression accelerates LDL cholesterol-mediated breast cancer growth in mouse models of hyperlipidemia. *Oncogene* **36**, 6462-6471 (2017).
11. Bahl, M.*, et al.* Serum lipids and outcome of early-stage breast cancer: results of a prospective cohort study. *Breast Cancer Res Treat* **94**, 135-144 (2005).
12. Rodrigues Dos Santos, C., Fonseca, I., Dias, S. & Mendes de Almeida, J.C. Plasma level of LDL-cholesterol at diagnosis is a predictor factor of breast tumor progression. *BMC Cancer* **14**, 132 (2014).
13. Wong, L.H., Gatta, A.T. & Levine, T.P. Lipid transfer proteins: the lipid commute via shuttles, bridges and tubes. *Nat Rev Mol Cell Biol* **20**, 85-101 (2019).
14. Cai, D.*, et al.* RORgamma is a targetable master regulator of cholesterol biosynthesis in a cancer subtype. *Nat Commun* **10**, 4621 (2019).
15. Shaitelman, S.F.*, et al.* Impact of Statin Use on Outcomes in Triple Negative Breast Cancer. *J Cancer* **8**, 2026-2032 (2017).
16. Smith, A., Murphy, L., Zgaga, L., Barron, T.I. & Bennett, K. Pre-diagnostic statin use, lymph node status and mortality in women with stages I-III breast cancer. *Br J Cancer* **117**, 588-596 (2017).
17. Prat, A. & Perou, C.M. Deconstructing the molecular portraits of breast cancer. *Mol Oncol* **5**, 5-23 (2011).
18. Badve, S.*, et al.* Basal-like and triple-negative breast cancers: a critical review with an emphasis on the implications for pathologists and oncologists. *Mod Pathol* **24**, 157-167 (2011).
19. Granit, R.Z.*, et al.* Regulation of Cellular Heterogeneity and Rates of Symmetric and Asymmetric Divisions in Triple-Negative Breast Cancer. *Cell Rep* **24**, 3237-3250 (2018).
20. Aw Yong, K.M.*, et al.* Heterogeneity at the invasion front of triple negative breast cancer cells. *Sci Rep* **10**, 5781 (2020).
21. Benayoun, B.A., Caburet, S. & Veitia, R.A. Forkhead transcription factors: key players in health and disease. *Trends Genet* **27**, 224-232 (2011).
22. Wang, Y., Zhou, Y. & Graves, D.T. FOXO transcription factors: their clinical significance and regulation. *Biomed Res Int* **2014**, 925350 (2014).
23. Willcox, B.J.*, et al.* FOXO3A genotype is strongly associated with human longevity. *Proc Natl Acad Sci U S A* **105**, 13987-13992 (2008).
24. Chen, Y.F.*, et al.* Synergistic effect of HIF-1alpha and FoxO3a trigger cardiomyocyte apoptosis under hyperglycemic ischemia condition. *J Cell Physiol* **233**, 3660-3671 (2018).
25. McClelland Descalzo, D.L.*, et al.* Glucose-Induced Oxidative Stress Reduces Proliferation in Embryonic Stem Cells via FOXO3A/beta-Catenin-Dependent Transcription of p21(cip1). *Stem Cell Reports* **7**, 55-68 (2016).
26. McGowan, S.E. & McCoy, D.M. Platelet-derived growth factor-A regulates lung fibroblast S-phase entry through p27(kip1) and FoxO3a. *Respir Res* **14**, 68 (2013).

27. Joseph, J.*, et al.* Inhibition of ROS and upregulation of inflammatory cytokines by FoxO3a promotes survival against Salmonella typhimurium. *Nat Commun* **7**, 12748 (2016).
28. Fluteau, A.*, et al.* The nuclear retention of transcription factor FOXO3a correlates with a DNA damage response and increased glutamine synthetase expression by astrocytes suggesting a neuroprotective role in the ageing brain. *Neurosci Lett* **609**, 11-17 (2015).
29. Kenyon, C.J. The genetics of ageing. *Nature* **464**, 504-512 (2010).
30. Liu, Y.*, et al.* Critical role of FOXO3a in carcinogenesis. *Mol Cancer* **17**, 104 (2018).
31. Yang, J.Y.*, et al.* ERK promotes tumorigenesis by inhibiting FOXO3a via MDM2-mediated degradation. *Nat Cell Biol* **10**, 138-148 (2008).
32. Guo, J.P.*, et al.* IKBKE phosphorylation and inhibition of FOXO3a: a mechanism of IKBKE oncogenic function. *PLoS One* **8**, e63636 (2013).
33. Chapuis, N.*, et al.* IkappaB kinase overcomes PI3K/Akt and ERK/MAPK to control FOXO3a activity in acute myeloid leukemia. *Blood* **116**, 4240-4250 (2010).
34. Zou, Y.*, et al.* Forkhead box transcription factor FOXO3a suppresses estrogen-dependent breast cancer cell proliferation and tumorigenesis. *Breast Cancer Res* **10**, R21 (2008).
35. Hu, M.C.*, et al.* IkappaB kinase promotes tumorigenesis through inhibition of forkhead FOXO3a. *Cell* **117**, 225-237 (2004).
36. Joung, J.*, et al.* Genome-scale CRISPR-Cas9 knockout and transcriptional activation screening. *Nat Protoc* **12**, 828-863 (2017).
37. Cheung, K.J.*, et al.* Polyclonal breast cancer metastases arise from collective dissemination of keratin 14-expressing tumor cell clusters. *Proc Natl Acad Sci U S A* **113**, E854-863 (2016).
38. Ma, S., Rao, L., Freedberg, I.M. & Blumenberg, M. Transcriptional control of K5, K6, K14, and K17 keratin genes by AP-1 and NF-kappaB family members. *Gene Expr* **6**, 361-370 (1997).
39. Ohkura, S.*, et al.* Complex formations involving both SP-1 and SP-3 at the transcriptional regulatory sequence correlate with the activation of the Keratin 14 gene in human oral squamous cell carcinoma cells. *Oncol Rep* **14**, 1577-1581 (2005).
40. Romano, R.A., Birkaya, B. & Sinha, S. A functional enhancer of keratin14 is a direct transcriptional target of deltaNp63. *J Invest Dermatol* **127**, 1175-1186 (2007).
41. Lopez, R.G.*, et al.* C/EBPalpha and beta couple interfollicular keratinocyte proliferation arrest to commitment and terminal differentiation. *Nat Cell Biol* **11**, 1181-1190 (2009).
42. Van Der Heide, L.P., Hoekman, M.F. & Smidt, M.P. The ins and outs of FoxO shuttling: mechanisms of FoxO translocation and transcriptional regulation. *Biochem J* **380**, 297-309 (2004).
43. Yin, L., Duan, J.J., Bian, X.W. & Yu, S.C. Triple-negative breast cancer molecular subtyping and treatment progress. *Breast Cancer Res* **22**, 61 (2020).
44. Karr, S. Epidemiology and management of hyperlipidemia. *Am J Manag Care* **23**, S139-S148 (2017).
45. Zaleska, M., Mozenska, O. & Bil, J. Statins use and cancer: an update. *Future Oncol* **14**, 1497-1509 (2018).
46. Ehmsen, S. & Ditzel, H.J. Signaling pathways essential for triple-negative breast cancer stem-like cells. *Stem Cells* **39**, 133-143 (2021).
47. Sousa, B.*, et al.* P-cadherin, vimentin and CK14 for identification of basal-like phenotype in breast carcinomas: an immunohistochemical study. *Histol Histopathol* **25**, 963-974 (2010).

48. Rastelli, F.*, et al.* Triple-negative breast cancer: current state of the art. *Tumori* **96**, 875-888 (2010).
49. Brunet, A.*, et al.* Akt promotes cell survival by phosphorylating and inhibiting a Forkhead transcription factor. *Cell* **96**, 857-868 (1999).
50. Lehtinen, M.K.*, et al.* A conserved MST-FOXO signaling pathway mediates oxidative-stress responses and extends life span. *Cell* **125**, 987-1001 (2006).
51. Kress, T.R.*, et al.* The MK5/PRAK kinase and Myc form a negative feedback loop that is disrupted during colorectal tumorigenesis. *Mol Cell* **41**, 445-457 (2011).
52. Shin, I., Bakin, A.V., Rodeck, U., Brunet, A. & Arteaga, C.L. Transforming growth factor beta enhances epithelial cell survival via Akt-dependent regulation of FKHRL1. *Mol Biol Cell* **12**, 3328-3339 (2001).
53. Chung, C.S., Huang, C.Y. & Chang, W. Vaccinia virus penetration requires cholesterol and results in specific viral envelope proteins associated with lipid rafts. *J Virol* **79**, 1623-1634 (2005).
54. Borst, J., Ahrends, T., Babala, N., Melief, C.J.M. & Kastenmuller, W. CD4(+) T cell help in cancer immunology and immunotherapy. *Nat Rev Immunol* **18**, 635-647 (2018).
55. Bennett, S.R., Carbone, F.R., Karamalis, F., Miller, J.F. & Heath, W.R. Induction of a CD8+ cytotoxic T lymphocyte response by cross-priming requires cognate CD4+ T cell help. *J Exp Med* **186**, 65-70 (1997).
56. Bennett, S.R.*, et al.* Help for cytotoxic-T-cell responses is mediated by CD40 signalling. *Nature* **393**, 478-480 (1998).
57. Schoenberger, S.P., Toes, R.E., van der Voort, E.I., Offringa, R. & Melief, C.J. T-cell help for cytotoxic T lymphocytes is mediated by CD40-CD40L interactions. *Nature* **393**, 480-483 (1998).
58. Konermann, S.*, et al.* Genome-scale transcriptional activation by an engineered CRISPR-Cas9 complex. *Nature* **517**, 583-588 (2015).
59. Chen, S.*, et al.* Genome-wide CRISPR screen in a mouse model of tumor growth and metastasis. *Cell* **160**, 1246-1260 (2015).
60. Doench, J.G.*, et al.* Rational design of highly active sgRNAs for CRISPR-Cas9-mediated gene inactivation. *Nat Biotechnol* **32**, 1262-1267 (2014).
61. Lee, G.Y., Kenny, P.A., Lee, E.H. & Bissell, M.J. Three-dimensional culture models of normal and malignant breast epithelial cells. *Nat Methods* **4**, 359-365 (2007).
62. Zuo, S.*, et al.* Enhanced antitumor efficacy of a novel oncolytic vaccinia virus encoding a fully monoclonal antibody against T-cell immunoglobulin and ITIM domain (TIGIT). *EBioMedicine* **64**, 103240 (2021).
63. Zhang, Y.*, et al.* Recombinant Adenovirus Expressing a Soluble Fusion Protein PD-1/CD137L Subverts the Suppression of CD8(+) T Cells in HCC. *Mol Ther* **27**, 1906-1918 (2019).

Figure Legends

Figure 1 Cholesterol metabolism was pivotal for TNBC progression.

a, Schematic representation of the in vivo screen using the mouse genome-scale CRISPR-Pool SAM library. 4T1 cells with genome-scale gene over-expression were generated, and inoculated s.c. into mice to allow tumor formation. Tumors were collected on days 5 and day 10 for sgRNA sequencing.

b, GO enrichment analysis of differential genes in tumor tissues between day 5 and day 10.

c, The survival analysis uses the data of BRCA patients provided by the TCGA.

d, 4T1 cells were inoculated subcutaneously (s.c.) into the BALB/c mice, and fed with high fat, high cholesterol or normal diet (n=7). The serum was collected on day 10 for cholesterol (CHOL) and LDL measurement.

e, The survival of mice received different diets were monitored.

f, Mice were sacrificed on day 14 (n=5). Lung and liver were collected for H&E staining (left). The metastatic nodes were counted (right). n.s., no significant difference; *p < 0.05, **p < 0.01; ***p < 0.001.

Figure 2 The effect of ApoA1 mediated cholesterol efflux on TNBC invasion.

a, The cholesterol levels in cytoplasm and supernatant were measured *in vitro*.

b, The $4T1^{WT}$ and $4T1^{ApoA1}$ cells were inoculated orthotopically into BALB/c mice (n=7). The tumor volume was monitored. Data were expressed as mean ±SD. c, The survival of mice was monitored. Mice lungs were collected on day 16 (n=5). Representative images are shown. Lung metastasis was indicated by black arrows (d). H&E staining of lung tissues (e).The lung metastasis were counted (f).

g, Cell clones of $4T1^{WT}$ or $4T1^{ApoA1}$ were cultured in matrigel and imaged at 24, 48 and 72 h.

h, Migration of $4T1^{WT}$ or $4T1^{ApoA1}$ was evaluated by wound healing assays.

i, Invasion of $4T1^{WT}$ or $4T1^{ApoA1}$ was evaluated by Transwell assays. Invasive cells were presented by with crystal violet staining (left), then crystal violet was reconstituted and absorbance was measured at 590 nm (right). *p < 0.05.

Figure 3 The effect of ApoA1 mediated cholesterol efflux on the expression of KRT14.

a, Volcano plots of the transcriptome comparison between $4T1^{WT}$ and $4T1^{ApoA1}$ cells.

b, GSEA enrichment of genes associated desmosome.

c, The expression of desmosome-related genes in $4T1^{WT}$ and $4T1^{ApoA1}$ cells.

d, KRT14 expression in tumor from patients with TNBC (n=299) or other type of breast cancers (nTNBC, n=1605). Data were collected from TCGA.

e, KRT14 expression in $4T1^{WT}$, $4T1^{ApoA1}$ (left), or HCC1937 transfected with or without ApoA1 encoding plasmid were determined by western blot.

f, The $4T1^{WT}$ and $4T1^{ApoA1}$ cells were inoculated orthotopically into BALB/c mice. Tumors were collected on day 7 for immunofluorescence analysis. red, KRT14; blue, nuclear.

g, 4T1ApoA1 cells were treated with or without 1mM of DIDS, and KRT14 expression were determined 24h later.

h, 4T1 with or without ABCA1 knock-down were transfected with ApoA1 over-expression plasmid, and KRT14 expression was determined 48h later.

i, KRT14 expression in 4T1ApoA1 was determined in the presence or absence of 2uM of cholesterol.

j, Tumors from mice fed with high fat, high CHOL or normal diet were collected for KRT14 detection on day 7.

k, The knock-down of KRT14 was determined by western blot.

l, The $4T1^{Ctr}$ and $4T1^{sh\text{-}KRT14}$ cells were inoculated orthotopically into BALB/c mice. Mice survival was monitored.

m, Lung tissues were collected on day 20.

n, 4T1ApoA1 cells were transfected with KRT14 encoding plasmid，and migration ability was determined by wound healing assays. *p < 0.05, **p < 0.01; ****p < 0.0001.

Figure 4 The role of FOXO3a in the cholesterol efflux induced KRT14 suppression.

a, mRNA level of KRT14 in $4T1^{WT}$, $4T1^{ApoA1}$ (left), or ApoA1 encoding plasmid transfected 4T1 (right) were determined by Q-PCR.

b, $4T1^{ApoA1}$ cells were transfected by the indicated siRNAs for 48h, mRNA level of KRT14 was determined by Q-PCR.

c, The expression of FOXO3a in tumors from patients with BRCA (Tumor) or normal mammary gland (Normal). Data were collected from TCGA.

d, $4T1^{ApoA1}$ cells were transfected with FOXO3a siRNA for 48h, KRT14 expression was determined by western blot.

e, $4T1^{ApoA1}$ cells were transfected with FOXO3a siRNA for 48h, and migration was determined by wound healing assays.

f, The plasmids in which the luciferase reporter gene was controlled by the truncated promoters of KRT14 were generated. $4T1^{WT}$ and $4T1^{ApoA1}$ cells were transfected with plasmids, and the luciferase activity was measured 48h later. -1~-2000, -1~-1500, -1~-800 and -1~-500 indicated the length of up-stream of transcription initiation site of KRT14. *p < 0.05.

g, The plasmids in which the luciferase reporter gene was controlled by mutant promoters of KRT14 were generated. 4T1ApoA1 cells were transfected with plasmids, and luciferase activity was measured 48h later. -879 ~ -872, -1716 ~ -1709, -1950 ~ -1943 and -1960 ~ -1953, represented the mutation sites. -1~-2000 WT is the wide type promoter of KRT14. **p < 0.01, compared with -1~-2000 WT.

h, CHIP-seq was performed in 4T1ApoA1 lysis by using Anti-FOXO3a. IGV analysis of CHIP-seq coverage was shown and the promoter region of KRT14 was indicated by the red arrow.

i, Immunohistochemical staining of KRT14 and FOXO3a in surgical breast cancer specimens. The representatives were shown.

j, Correlation analysis of the expression between FOXO3a and KRT14, serum ApoA1 or serum HDL from patients with breast cancer.

Figure 5 The role of IKK pathway in ApoA1 mediated nuclear translocation of FOXO3a.

a, The level of nuclear FOXO3a in 4T1 or HCC1937 cells with or without ApoA1 over-expression.

b, 4T1 and HCC1937 were transfected with ApoA1 expressing plasmid or control plasmid. Phosphorylation of Akt, FOXO3a (S315 site) and IkB was detected by western blot.

c, Tumors were collected from mice orthotopically inoculated with $4T1^{WT}$ or $4T1^{ApoA1}$ cells for the measurement of phosphorylated p65.

d, The mRNA level of CHUK, IKBKB, IKBKE and IKBKG in $4T1^{WT}$ and $4T1^{ApoA1}$ cells. CHUK, component of inhibitor of nuclear factor Kappa B kinase complex; IKBKB, inhibitor of nuclear factor Kappa B kinase subunit beta; IKBKE, inhibitor of nuclear factor Kappa B kinase subunit epsilon; IKBKG, inhibitor of nuclear factor Kappa B kinase subunit gamma. $^{**}p < 0.01$, $^{***}p < 0.001$.

e, The expression of KRT14 in $4T1^{ApoA1}$ cells transfected with IKBKB, IKBKE or IKBKG encoding plasmids.

f, The level of nuclear FOXO3a in $4T1^{WT}$ and $4T1^{ApoA1}$ cells transfected with flag conjugated WT, Akt-mut, ERK-mut or IKK-mut FOXO3a encoding plasmid. WT, wild type of FOXO3a; Akt-mut, FOXO3a with mutation in Akt phosphorylation sites； ERK-mut, FOXO3a with mutation in ERK phosphorylation sites; IKK-mut, FOXO3a with a mutation in IKK phosphorylation site.

Figure 6 The anti-tumor effect of adenovirus-vector based ApoA1 gene therapy.

a, The breast cancer orthotopic model was established by implantation of 5×10^5 4T1 cells on the fourth mammary gland of BALB/c mice. When the tumor volume reached approximately 100 mm3 (day 0), the tumor-bearing mice were treated with saline, 5×10^8 PFU of ADV-Ctr,

or ADV-ApoA1 at a 2-day interval for 3 times via intratumoral injection. Tumor volume and mice survival were monitored. n.s., no significance;

b, The breast cancer subcutaneous model was established by implantation of 5 x 10^5 4T1 cells on the right flank of BALB/c mice. When the tumor volume reached approximately 100 mm3 (day 0), the tumor-bearing mice received the intratumoral injection with saline, 1 x 10^{11} v.g. of AAV-Control, or AAV-ApoA1. Mice received a second AAV injection on day 7. Tumor volume and mice survival were monitored. n.s., no significance; *$p < 0.05$.

c, The breast cancer orthotopic model was established with luciferase expressing 4T1 cells. Primary tumors were removed by surgical resection. Tumor metastasis was monitored by bioluminescence analysis on day 40.

d, Mice with orthotopic breast cancer 4T1 were treated twice with saline, 5 x 10^8 PFU of ADV-Ctr, or ADV-ApoA1. Tumors were collected 48h after the last injection. mRNA level of KRT14 was determined by Q-PCR.

e, 4T1 cells were infected with ADV-Ctr, or ADV-ApoA1 at MOI=10 *in vitro*. KRT14 expression was determined by western blot.

f, 4T1 and HCC1937 cells were transfected with E1A encoding plasmid in vitro, and the mRNA level of ABCA1 was determined by Q-PCR.

g, Tumors were collected from 4T1 bearing mice received with ADV or AAV treatment for transcriptome analysis. The level of the different immune cell populations in TME was determined by ssGSEA.

h, GSEA enrichment of RNA-seq data from ADV-Ctr, or ADV-ApoA1 treated primary tumors.

i, GSEA enrichment of RNA-seq data from $4T1^{WT}$ and $4T1^{ApoA1}$ cells.

j, The expression of MHC I and MHC II on $4T1^{WT}$ and $4T1^{ApoA1}$ cells were measured by flow cytometry. *$p < 0.05$, **$p < 0.01$, ***$p < 0.01$.

k, A schematic overview of the mechanisms involved in the ADV-ApoA1 mediated tumor suppression. With the treatment of ADV-ApoA1, the adenovirus protein E1A leads to an up-regulation of the receptor ABCA1, which facilitates the cholesterol efflux in the presence of elevated ApoA1 production. The decrease of intracellular cholesterol impairs the activity of IKK pathway, causing the de-phosphorylation of FOXO3a. Dephosphorylated FOXO3a translocates into the nuclear and directly binds to the promoter region of KRT14 to inhibit its transcription. The down-regulated expression of KRT14 in TNBC leads to an attenuated metastasis and elicits anti-tumor immune responses.

Figures

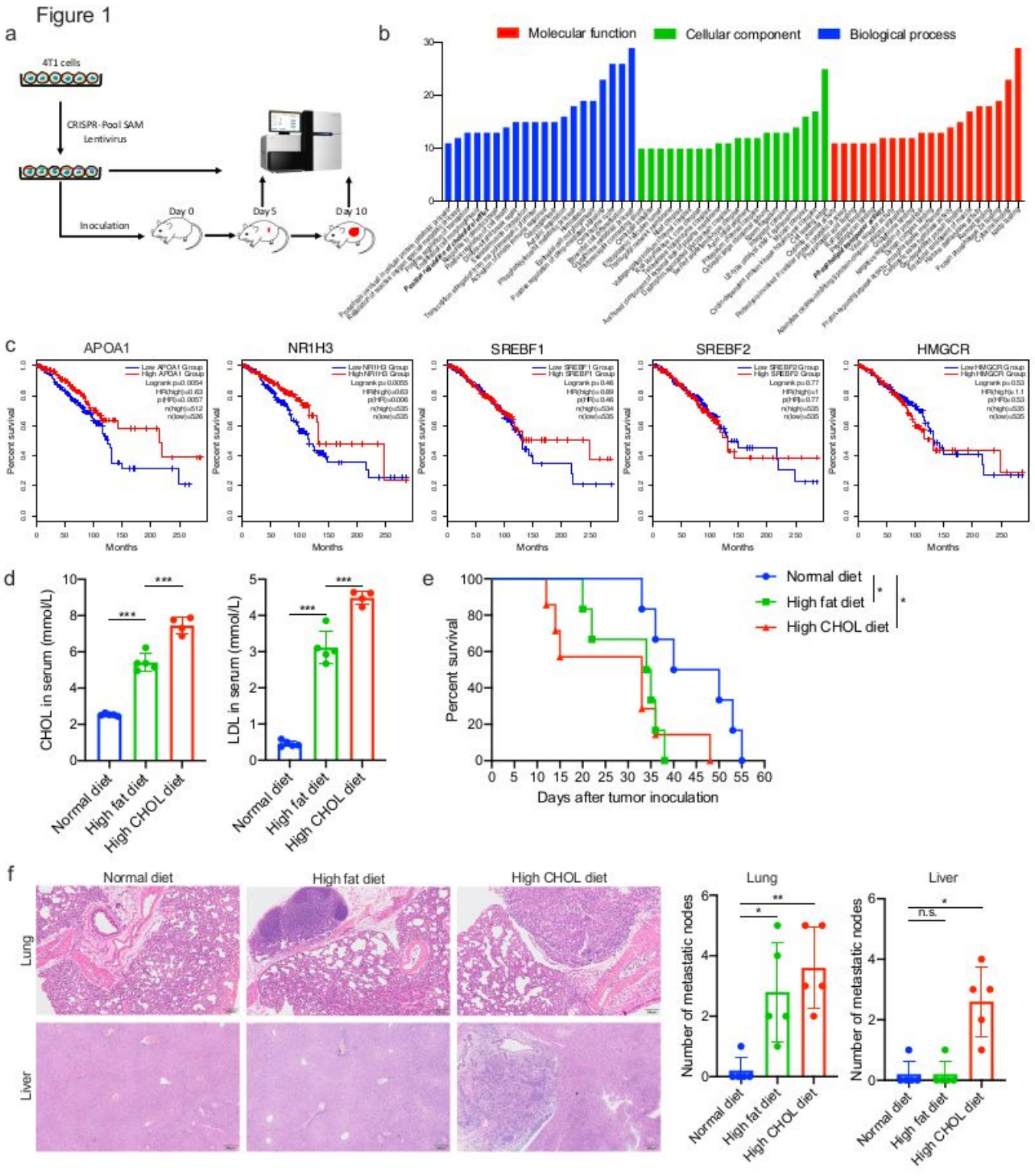

Figure 1

Cholesterol metabolism was pivotal for TNBC progression. a, Schematic representation of the in vivo screen using the mouse genome-scale CRISPR-Pool SAM library. 4T1 cells with genome-scale gene over-expression were generated, and inoculated s.c. into mice to allow tumor formation. Tumors were collected

on days 5 and day 10 for sgRNA sequencing. b, GO enrichment analysis of differential genes in tumor tissues between day 5 and day 10. c, The survival analysis uses the data of BRCA patients provided by the TCGA. d, 4T1 cells were inoculated subcutaneously (s.c.) into the BALB/c mice, and fed with high fat, high cholesterol or normal diet (n=7). The serum was collected on day 10 for cholesterol (CHOL) and LDL measurement. e, The survival of mice received different diets were monitored. f, Mice were sacrificed on day 14 (n=5). Lung and liver were collected for H□E staining (left). The metastatic nodes were counted (right). n.s., no significant difference; *p < 0.05, **p < 0.01; ***p < 0.001.

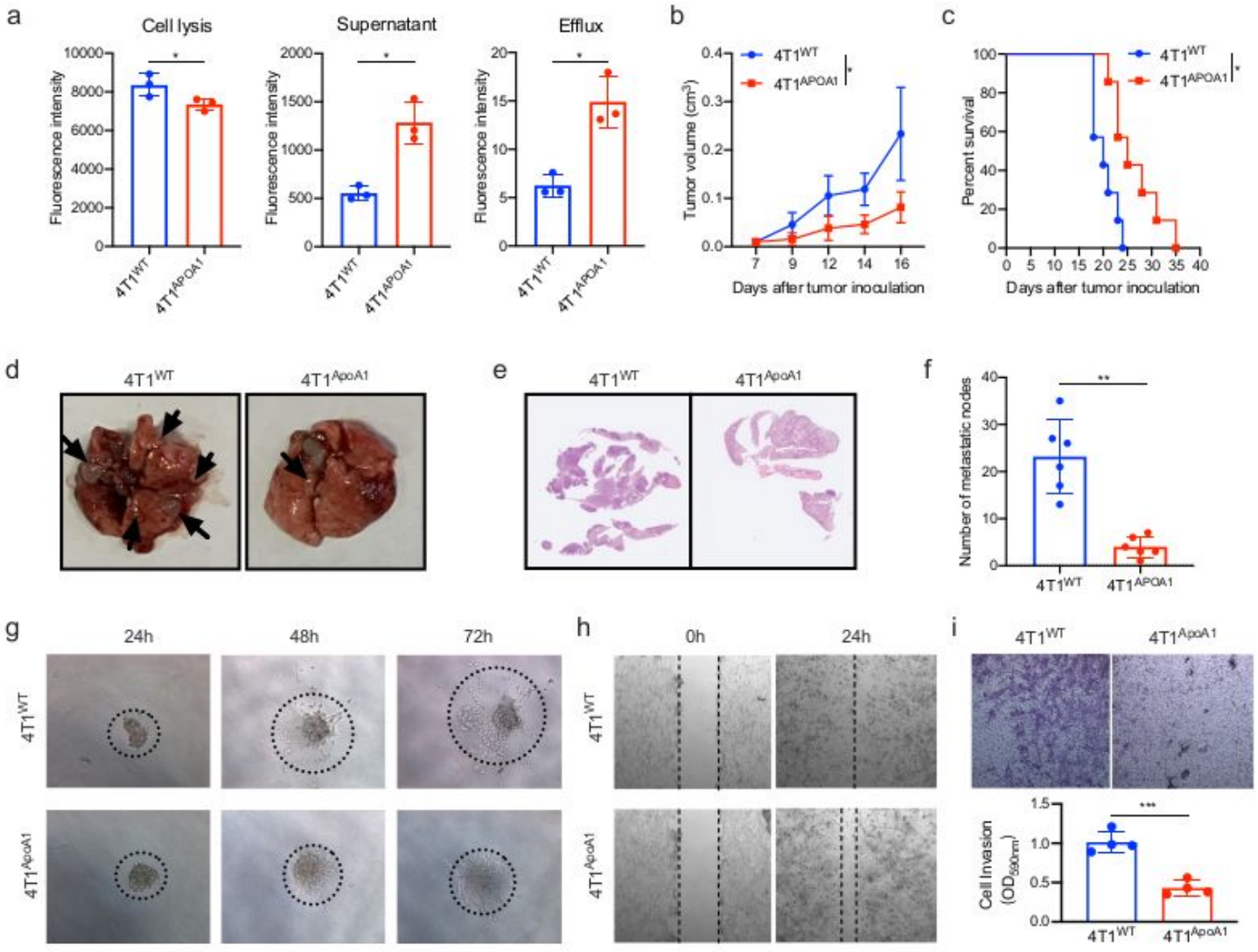

Figure 2

Figure 2

The effect of ApoA1 mediated cholesterol efflux on TNBC invasion. a, The cholesterol levels in cytoplasm and supernatant were measured in vitro. b, The 4T1WT and 4T1ApoA1 cells were inoculated orthotopically into BALB/c mice (n=7). The tumor volume was monitored. Data were expressed as mean ±SD. c, The survival of mice was monitored. Mice lungs were collected on day 16 (n=5). Representative

images are shown. Lung metastasis was indicated by black arrows (d). H&E staining of lung tissues (e).The lung metastasis were counted (f). g, Cell clones of 4T1WT or 4T1ApoA1 were cultured in matrigel and imaged at 24, 48 and 72 h. h, Migration of 4T1WT or 4T1ApoA1 was evaluated by wound healing assays. i, Invasion of 4T1WT or 4T1ApoA1 was evaluated by Transwell assays. Invasive cells were presented by with crystal violet staining (left), then crystal violet was reconstituted and absorbance was measured at 590 nm (right). *p < 0.05.

Figure 3

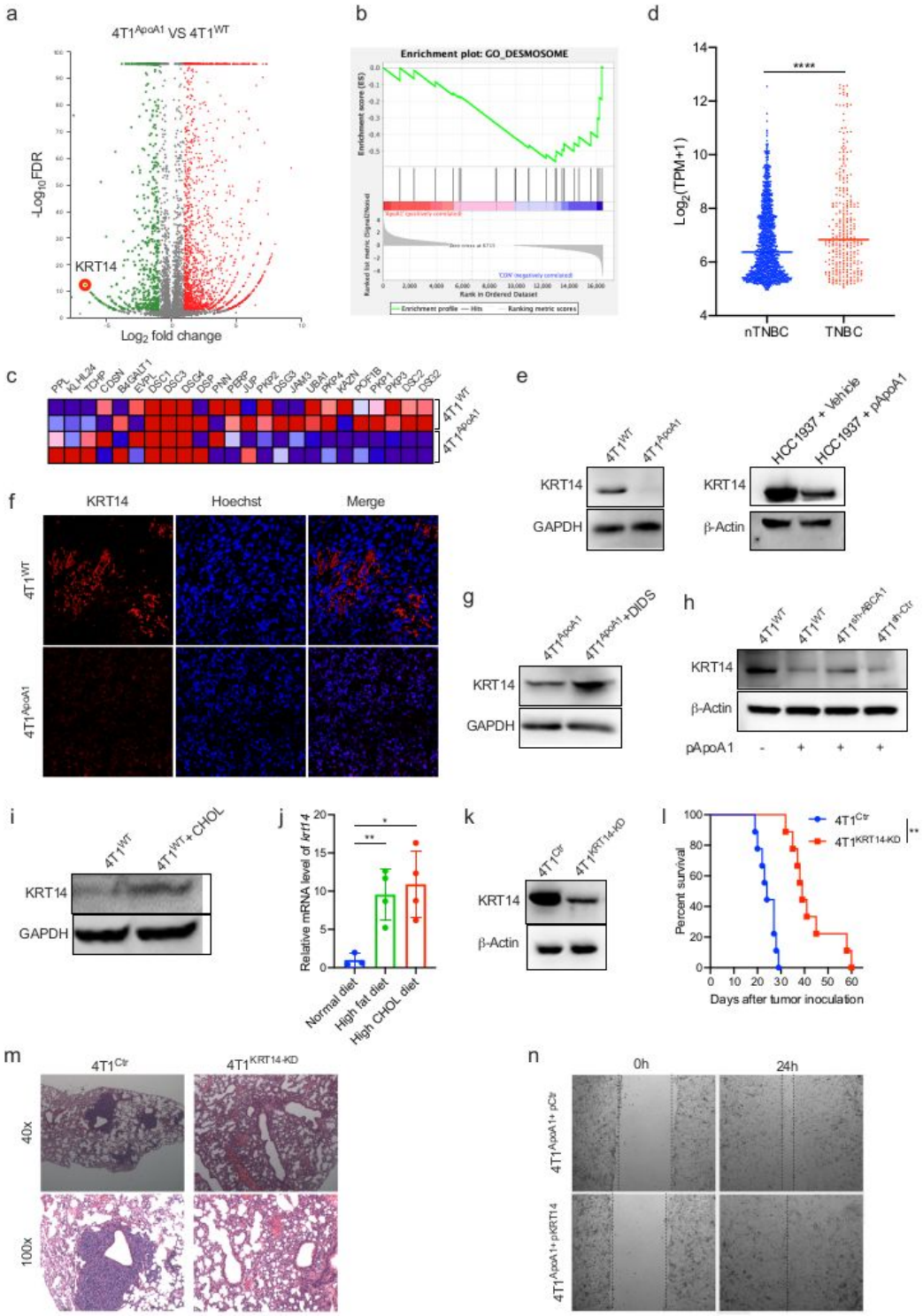

Figure 3

The effect of ApoA1 mediated cholesterol efflux on the expression of KRT14. a, Volcano plots of the transcriptome comparison between 4T1WT and 4T1ApoA1 cells. b, GSEA enrichment of genes associated desmosome. c, The expression of desmosome-related genes in 4T1WT and 4T1ApoA1 cells. d, KRT14 expression in tumor from patients with TNBC (n=299) or other type of breast cancers (nTNBC, n=1605). Data were collected from TCGA. e, KRT14 expression in 4T1WT, 4T1ApoA1 (left), or HCC1937 transfected with or without ApoA1 encoding plasmid were determined by western blot. f, The 4T1WT and 4T1ApoA1 cells were inoculated orthotopically into BALB/c mice. Tumors were collected on day 7 for immunofluorescence analysis. red, KRT14; blue, nuclear. g, 4T1ApoA1 cells were treated with or without 1mM of DIDS, and KRT14 expression were determined 24h later. h, 4T1 with or without ABCA1 knock-down were transfected with ApoA1 over-expression plasmid, and KRT14 expression was determined 48h later. i, KRT14 expression in 4T1ApoA1 was determined in the presence or absence of 2uM of cholesterol. j, Tumors from mice fed with high fat, high CHOL or normal diet were collected for KRT14 detection on day 7. k, The knock-down of KRT14 was determined by western blot. l, The 4T1Ctr and 4T1sh-KRT14 cells were inoculated orthotopically into BALB/c mice. Mice survival was monitored. m, Lung tissues were collected on day 20. n, 4T1ApoA1 cells were transfected with KRT14 encoding plasmid and migration ability was determined by wound healing assays. *p < 0.05, **p < 0.01; ****p < 0.0001.

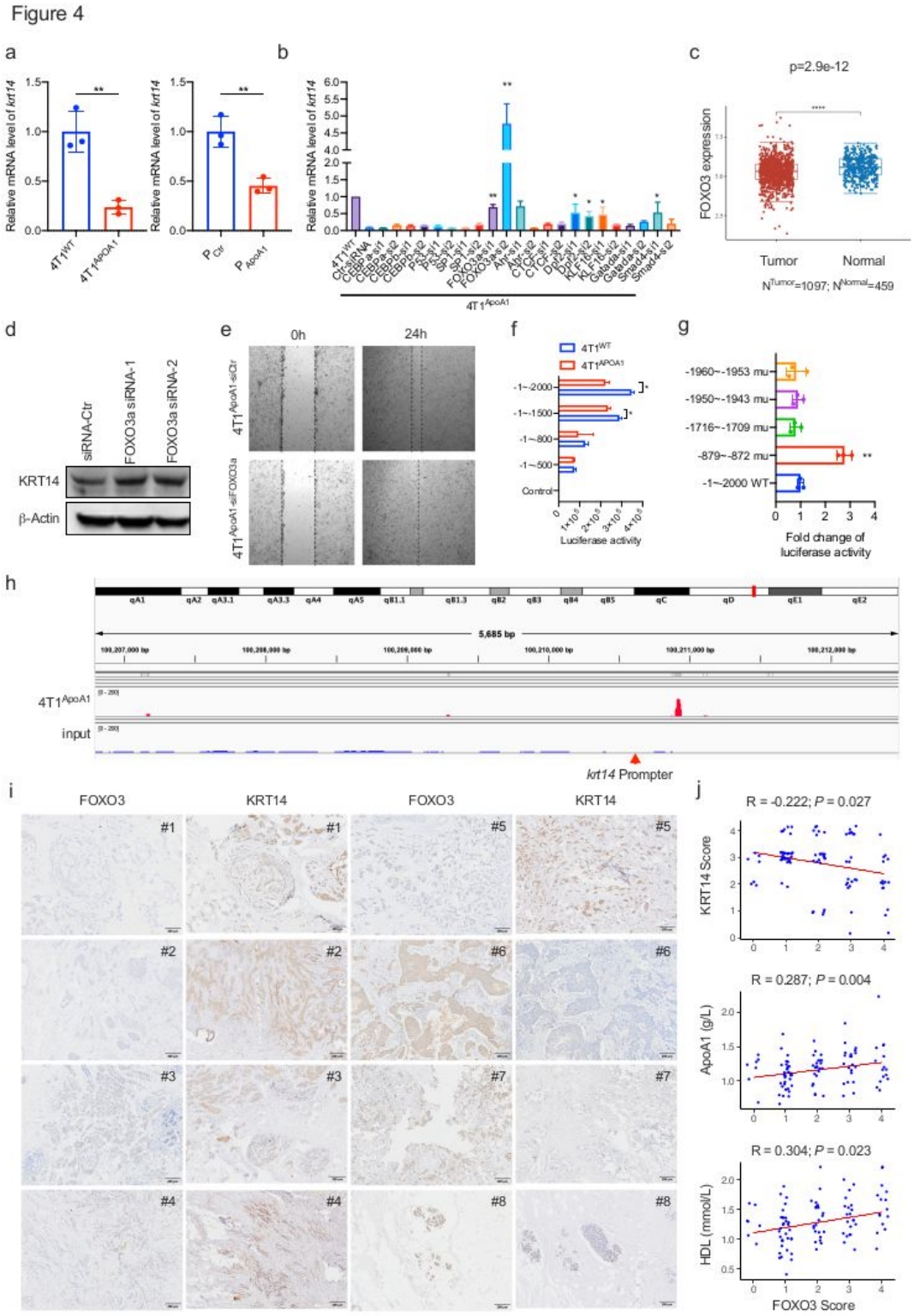

Figure 4

The role of FOXO3a in the cholesterol efflux induced KRT14 suppression. a, mRNA level of KRT14 in 4T1WT, 4T1ApoA1 (left), or ApoA1 encoding plasmid transfected 4T1 (right) were determined by Q-PCR. b, 4T1ApoA1 cells were transfected by the indicated siRNAs for 48h, mRNA level of KRT14 was determined by Q-PCR. c, The expression of FOXO3a in tumors from patients with BRCA (Tumor) or normal mammary gland (Normal). Data were collected from TCGA. d, 4T1ApoA1 cells were transfected with

FOXO3a siRNA for 48h, KRT14 expression was determined by western blot. e, 4T1ApoA1 cells were transfected with FOXO3a siRNA for 48h, and migration was determined by wound healing assays. f, The plasmids in which the luciferase reporter gene was controlled by the truncated promoters of KRT14 were generated. 4T1WT and 4T1ApoA1 cells were transfected with plasmids, and the luciferase activity was measured 48h later. -1~-2000, -1~-1500, -1~-800 and -1~-500 indicated the length of up-stream of transcription initiation site of KRT14. *p < 0.05. g, The plasmids in which the luciferase reporter gene was controlled by mutant promoters of KRT14 were generated. 4T1ApoA1 cells were transfected with plasmids, and luciferase activity was measured 48h later. -879 ~ -872, -1716 ~ -1709, -1950 ~ -1943 and -1960 ~ - 1953, represented the mutation sites. -1~-2000 WT is the wide type promoter of KRT14. **p < 0.01, compared with -1~-2000 WT. h, CHIP-seq was performed in 4T1ApoA1 lysis by using Anti-FOXO3a. IGV analysis of CHIP-seq coverage was shown and the promoter region of KRT14 was indicated by the red arrow. i, Immunohistochemical staining of KRT14 and FOXO3a in surgical breast cancer specimens. The representatives were shown. j, Correlation analysis of the expression between FOXO3a and KRT14, serum ApoA1 or serum HDL from patients with breast cancer.

Figure 5

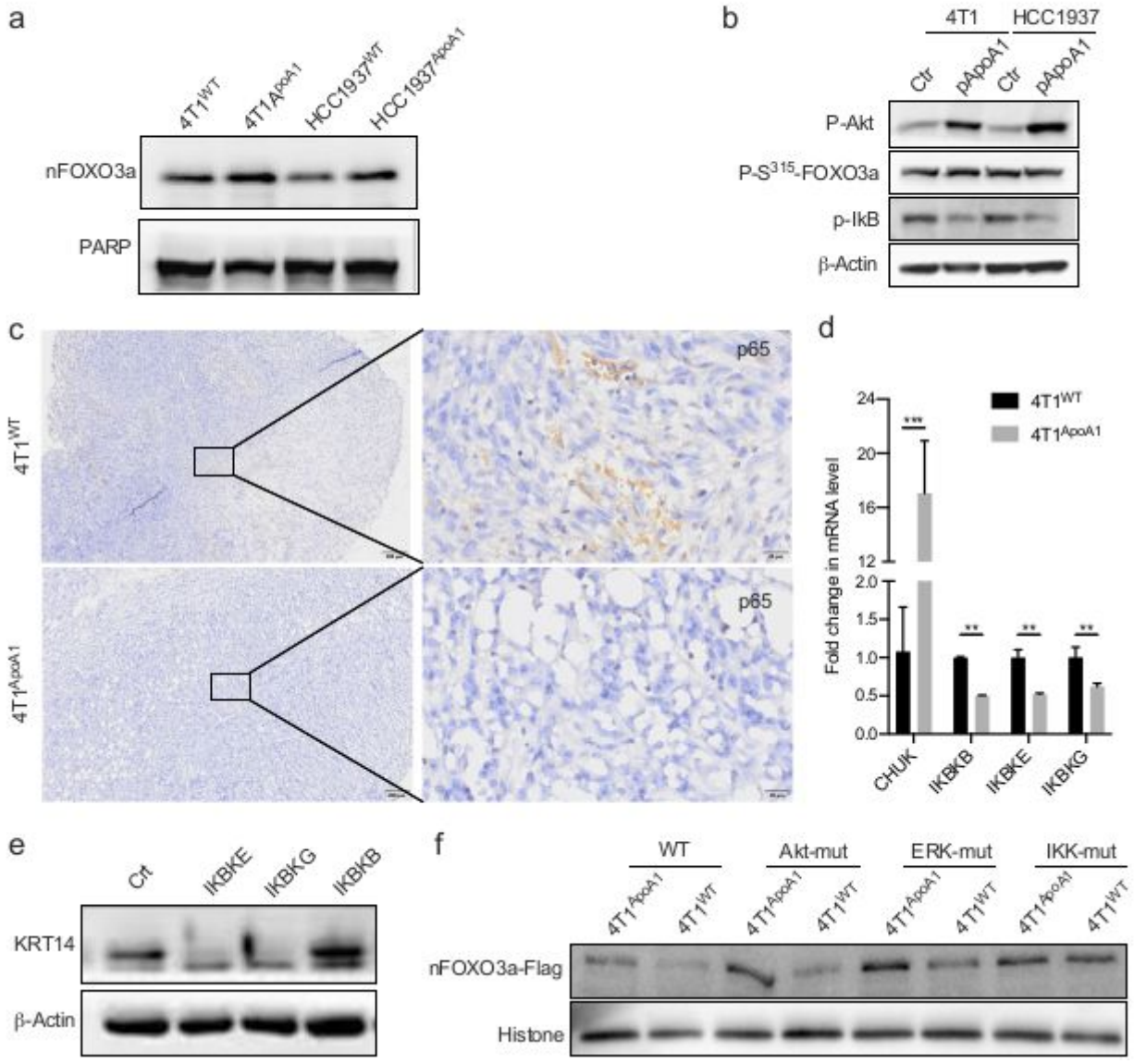

Figure 5

The role of IKK pathway in ApoA1 mediated nuclear translocation of FOXO3a. a, The level of nuclear FOXO3a in 4T1 or HCC1937 cells with or without ApoA1 overexpression. b, 4T1 and HCC1937 were transfected with ApoA1 expressing plasmid or control plasmid. Phosphorylation of Akt, FOXO3a (S315 site) and IkB was detected by western blot. c, Tumors were collected from mice orthotopically inoculated with 4T1WT or 4T1ApoA1 cells for the measurement of phosphorylated p65. d, The mRNA level of CHUK, IKBKB, IKBKE and IKBKG in 4T1WT and 4T1ApoA1 cells. CHUK, component of inhibitor of nuclear factor Kappa B kinase complex; IKBKB, inhibitor of nuclear factor Kappa B kinase subunit beta; IKBKE, inhibitor of nuclear factor Kappa B kinase subunit epsilon; IKBKG, inhibitor of nuclear factor Kappa B kinase subunit gamma. **p < 0.01, ***p < 0.001. e, The expression of KRT14 in 4T1ApoA1 cells transfected with IKBKB, IKBKE or IKBKG encoding plasmids. f, The level of nuclear FOXO3a in 4T1WT and 4T1ApoA1 cells

transfected with flag conjugated WT, Akt-mut, ERK-mut or IKK-mut FOXO3a encoding plasmid. WT, wild type of FOXO3a; Akt-mut, FOXO3a with mutation in Akt phosphorylation sites；ERK-mut, FOXO3a with mutation in ERK phosphorylation sites; IKK-mut, FOXO3a with a mutation in IKK phosphorylation site.

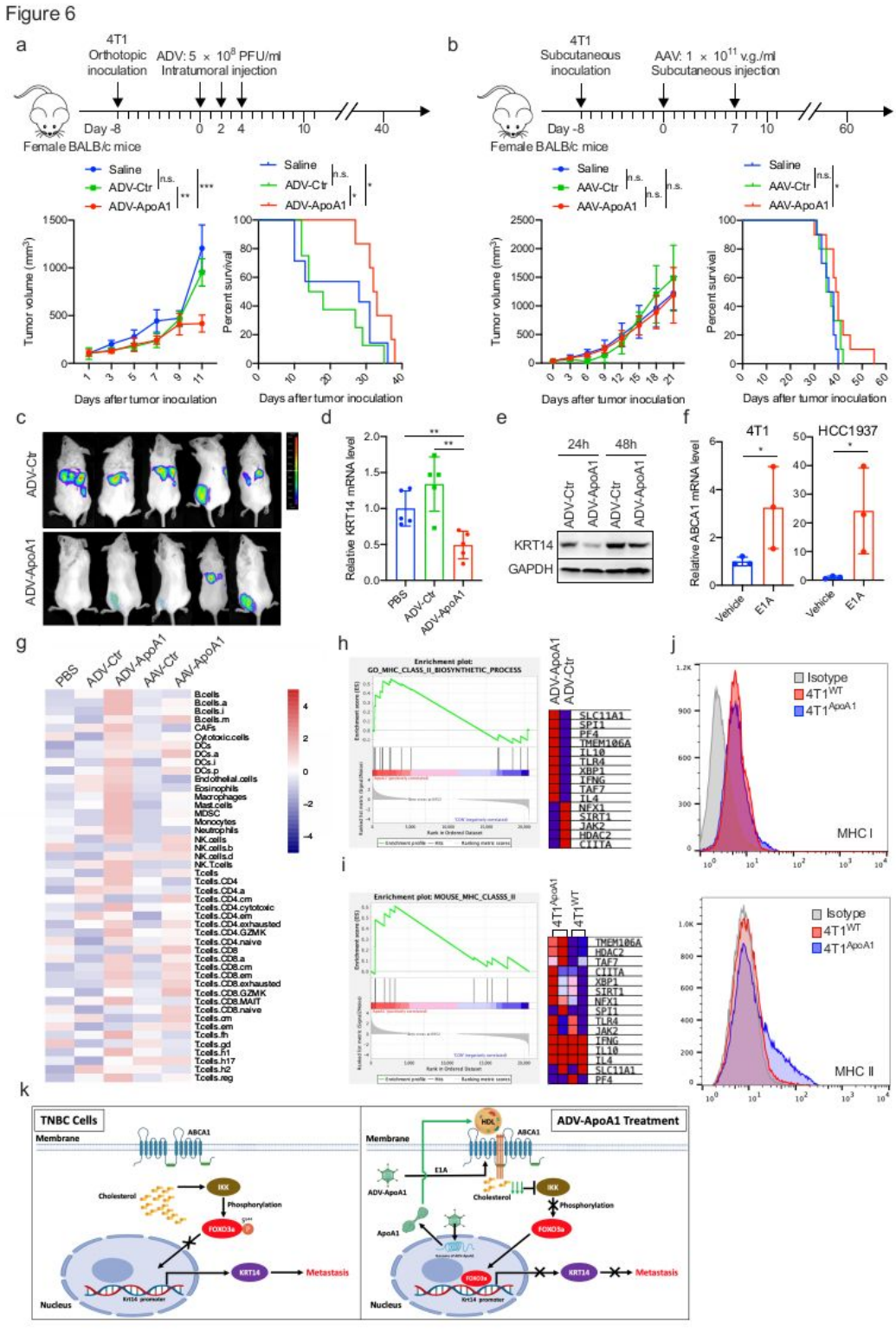

Figure 6

The anti-tumor effect of adenovirus-vector based ApoA1 gene therapy. a, The breast cancer orthotopic model was established by implantation of 5 x 105 4T1 cells on the fourth mammary gland of BALB/c

mice. When the tumor volume reached approximately 100 mm3 (day 0), the tumor-bearing mice were treated with saline, 5 x 108 PFU of ADV-Ctr, or ADV-ApoA1 at a 2-day interval for 3 times via intratumoral injection. Tumor volume and mice survival were monitored. n.s., no significance; b, The breast cancer subcutaneous model was established by implantation of 5 x 105 4T1 cells on the right flank of BALB/c mice. When the tumor volume reached approximately 100 mm3 (day 0), the tumor-bearing mice received the intratumoral injection with saline, 1 x 1011 v.g. of AAV-Control, or AAV-ApoA1. Mice received a second AAV injection on day 7. Tumor volume and mice survival were monitored. n.s., no significance; *p < 0.05. c, The breast cancer orthotopic model was established with luciferase expressing 4T1 cells. Primary tumors were removed by surgical resection. Tumor metastasis was monitored by bioluminescence analysis on day 40. d, Mice with orthotopic breast cancer 4T1 were treated twice with saline, 5 x 108 PFU of ADVCtr, or ADV-ApoA1. Tumors were collected 48h after the last injection. mRNA level of KRT14 was determined by Q-PCR. e, 4T1 cells were infected with ADV-Ctr, or ADV-ApoA1 at MOI=10 in vitro. KRT14 expression was determined by western blot. f, 4T1 and HCC1937 cells were transfected with E1A encoding plasmid in vitro, and the mRNA level of ABCA1 was determined by Q-PCR. g, Tumors were collected from 4T1 bearing mice received with ADV or AAV treatment for transcriptome analysis. The level of the different immune cell populations in TME was determined by ssGSEA. h, GSEA enrichment of RNA-seq data from ADV-Ctr, or ADV-ApoA1 treated primary tumors. i, GSEA enrichment of RNA-seq data from 4T1WT and 4T1ApoA1 cells. j, The expression of MHC I and MHC II on 4T1WT and 4T1ApoA1 cells were measured by flow cytometry. *p < 0.05, **p < 0.01, ***p < 0.01. k, A schematic overview of the mechanisms involved in the ADV-ApoA1 mediated tumor suppression. With the treatment of ADV-ApoA1, the adenovirus protein E1A leads to an upregulation of the receptor ABCA1, which facilitates the cholesterol efflux in the presence of elevated ApoA1 production. The decrease of intracellular cholesterol impairs the activity of IKK pathway, causing the de-phosphorylation of FOXO3a. Dephosphorylated FOXO3a translocates into the nuclear and directly binds to the promoter region of KRT14 to inhibit its transcription. The down-regulated expression of KRT14 in TNBC leads to an attenuated metastasis and elicits anti-tumor immune responses.

Supplementary Files

This is a list of supplementary files associated with this preprint. Click to download.

- FigureS1.pdf
- FigureS2.pdf
- FigureS3.pdf
- FigureS4.pdf
- FigureS5.pdf